Letter

Hyperbolic plasmons in massive tilted two-dimensional Dirac materials

M. A. Mojarro [1,2] R. Carrillo-Bastos [2] and Jesús A. Maytorena [3,*]

[1]*Department of Physics and Astronomy, Ohio University, Athens, Ohio 45701, USA*
[2]*Facultad de Ciencias, Universidad Autónoma de Baja California, Apartado Postal 1880, 22800 Ensenada, Baja California, México*
[3]*Centro de Nanociencias y Nanotecnología, Universidad Nacional Autónoma de México,*
Apartado Postal 2681, 22800 Ensenada, Baja California, México

We explore topological transitions in the type of propagation of surface electromagnetic modes in massive anisotropic tilted two-dimensional (2D) Dirac systems. The presence of tilting and mass gives rise to an indirect band gap that strongly modifies the joint density of states compared to the gapless system. New Van Hove singularities appear, and the interplay between intra- and interband transitions leads to an anisotropic optical conductivity with imaginary parts acquiring opposite signs in orthogonal directions, opening the possibility of having hyperbolic propagation of plasmons. Isofrequency contours and low plasmon losses, as obtained from the dispersion relation, show that transitions between purely anisotropic quasielliptical and well-defined, highly directional, hyperbolic modes are attainable only when tilt and mass coexist via frequency and Fermi level variation. This behavior could be probed in massive tilted 2D Dirac materials like the organic-layered compound α-(BEDT-TTF)$_2$I$_3$ [BEDT-TTF = (bis-(ethylenedithio)tetrathiafulvalene)] or WTe$_2$, in which hyperbolic plasmons were recently observed, through far-infrared absorption, optical nanoscopy, and similar current tools in graphene plasmonics.

The recent emergence of natural two-dimensional (2D) hyperbolic materials [1,2] offers a way to circumvent the fabrication challenges of hyperbolic metasurfaces [3] and the constrictions on the dispersion relation that lead to sizable structural periodicity [4]. Moreover, these 2D materials have shown hyperbolic plasmonic behavior in a wide range of frequencies from midinfrared to UV, accompanied by high tunability with doping and gating [5]. For example, experiments on thin films of WTe$_2$ demonstrated a hyperbolic frequency range of 13–18 THz [6] originating from in-plane intraband anisotropic transitions [7], and first-principles calculations showed a second window around 241 THz, associated with resonant anisotropic interband transitions via band nesting [8]. In contrast, MoTe$_2$, another transition-metal telluride, is a natural hyperbolic material with low losses across the visible and ultraviolet regions [9] (725–1450 THz). Still, the hyperbolicity condition now relies upon the in-plane and out-of-plane components of the dielectric tensor. Similar mechanisms are behind the indefinite behavior of electride materials [10] and Van der Waals crystals [11] that present hyperbolic windows in the infrared and layered hexagonal crystals [12] that are hyperbolic in the visible and UV range. Other examples of two-dimensional hyperbolic materials include black phosphorous, with two hyperbolic windows [13,14] in the infrared (80 THz) and visible (677 THz) ranges; carbon phosphide [15], which is hyperbolic in the infrared; and 8-*Pmmn* borophene [16], MoOCl$_2$ [17], and nodal-line semimetals [18,19]. In all these systems, hyperbolicity results from the intrinsic anisotropic arrangement of atoms in the

material and its corresponding anisotropic interplay of intra- and interband optical responses. Therefore, typical isotropic Dirac materials like graphene do not display hyperbolic plasmons; even with anisotropic Fermi velocity [20] or tilting [21], the low-loss plasmon dispersion for these materials is still elliptical. However, in a recent study, we showed that massive tilted Dirac systems, like the metal-organic (which consists of alternatively conducting layers of BEDT-TTF (bis-(ethylenedithio)tetrathiafulvalene) molecules and insulating layers of tri-iodine anions) [22,23], present a directional optical response due to the combination of tilting and gap [24], thus opening the possibility of hosting low-loss hyperbolic plasmons for Dirac materials. Consequently, in this Letter, we report a scenario of hyperbolic propagation in 2D Dirac systems involving tilt *and* mass (in the tens of terahertz) and show that if one of these elements is absent, plasmon propagation is strictly the purely anisotropic elliptic type, without any transition to a hyperbolic regime.

We consider a 2D gapped anisotropic Dirac system with the low-energy Hamiltonian [24–27]

$$H_\xi(\mathbf{k}) = \xi(\hbar v_t k_y \mathbb{1} + \hbar v_x k_x \sigma_x + \xi \hbar v_y k_y \sigma_y) + \Delta \sigma_z, \quad (1)$$

where σ_i are Pauli matrices defined in the pseudospin space, the carrier velocities v_x and v_y account for the anisotropy of the model, and $\mathbf{k} = k_x \hat{\mathbf{x}} + k_y \hat{\mathbf{y}}$ is the electron wave vector for states in the vicinity of the K (K') point with valley index $\xi = + (-)$; $\mathbb{1}$ is the 2×2 identity matrix. The system includes a mass $\Delta > 0$ in each valley and an amount of tilting ξv_t along the k_y axis. In the absence of mass, the model describes some 2D graphenelike materials and organic conductors [21,28–30]. Taking $v_x = v_y = v_F$ reduces Eq. (1) to the graphene Hamiltonian, while the 8-*Pmmn* borophene Hamiltonian is
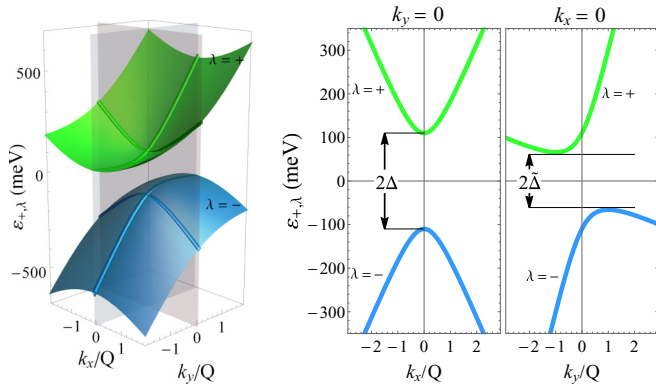
*jesusm@ens.cnyn.unam.mx

FIG. 1. Energy bands at a $\xi = +$ valley of a massive tilted Dirac system and two cuts with planes $k_y = 0$ and $k_x = 0$. Along the k_x axis the bands are separated by 2Δ, but along the k_y axis the system presents the minimum separation $2\tilde{\Delta}$ ($<2\Delta$), which is of indirect nature. This represents an additional source of anisotropy and modifies the interplay between intra- and interband contributions to the optical response.

recovered with the values [31] $v_x = 0.86 v_F$, $v_y = 0.69 v_F$, and $v_t = 0.32 v_F$, with $v_F = 10^6$ m/s. A realistic example of the complete model is the organic conductor α-(BEDT-TTF)$_2$I$_3$, a well-recognized 2D massive Dirac fermion system with a pair of tilted Dirac cones under hydrostatic pressure close to a critical pressure [23,32–34]. Recently, a Hamiltonian similar to (1) was derived from an eight-band model for monolayer WTe$_2$ near the Dirac points [35], with $v_x = 0.644 \times 10^6$ m/s, $v_y = 0.365 \times 10^6$ m/s, and $v_t = 0.463 \times 10^6$ m/s. It is in this material that natural hyperbolic plasmons have been measured [6]. Moreover, our model will also apply to 8-*Pmmn* borophene if a band gap is opened by hydrogenation, as recently predicted [36].

The energy-momentum dispersion reads

$$\varepsilon_{\xi,\lambda}(k_x, k_y) = \xi \alpha_t k_y + \lambda \sqrt{\alpha_x^2 k_x^2 + \alpha_y^2 k_y^2 + \Delta^2}, \quad (2)$$

where $\alpha_i = \hbar v_i$ ($i = x, y, t, F$) and the index $\lambda = \pm$ labels the conduction ($\lambda = +$) and the valence ($\lambda = -$) bands in each valley $\xi = \pm$. A distinctive feature of the model is that the simultaneous presence of tilt and mass produces an indirect gap in each valley around the nominal Dirac point [26] (Fig. 1). Indeed, the conduction branches $\varepsilon_{\xi,+}(\mathbf{k})$ present a minimum at $\mathbf{k} = -\xi Q \hat{\mathbf{y}}$, while the valence branches $\varepsilon_{\xi,-}(\mathbf{k})$ display a maximum at $\mathbf{k} = +\xi Q \hat{\mathbf{y}}$, where $\alpha_y Q = \Delta(\gamma/\sqrt{1-\gamma^2})$, with the tilting parameter $\gamma = v_t/v_y$ ($0 \leqslant \gamma < 1$). Thus, a Fermi level within the gap reads $\varepsilon_F < \tilde{\Delta}$, where $\tilde{\Delta} = \Delta\sqrt{1-\gamma^2} < \Delta$. This means that a new scenario is possible with the Fermi level lying in the "indirect zone" $\tilde{\Delta} < \varepsilon_F < \Delta$. This has a striking effect on the spectrum of interband transitions [24]. (1) For the Fermi level within the gap, the joint density of states (JDOS) displays a graphenelike linear dependence on the exciting energy $\hbar\omega$ above the threshold of 2Δ, but involving the geometric mean velocity $\sqrt{v_x v_y}$ instead of Fermi velocity v_F. (2) On the other hand, for $\varepsilon_F > \Delta$, the absence of particle-hole symmetry leads to the appearance of two critical energies,

$$\hbar\omega_\pm = 2[\varepsilon_F \pm \gamma \sqrt{\varepsilon_F^2 - \tilde{\Delta}^2}]/(1-\gamma^2), \quad (3)$$
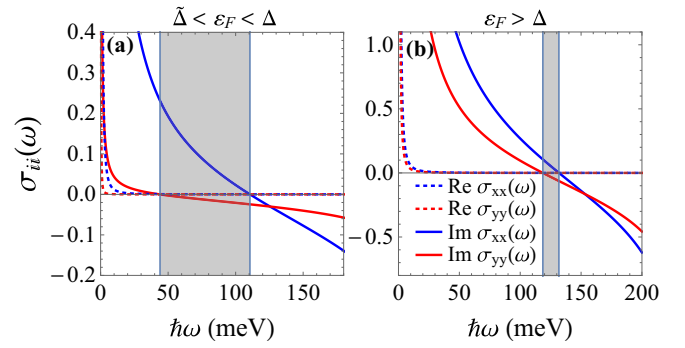

FIG. 2. Optical conductivities $\sigma_{xx}(\omega)$ and $\sigma_{yy}(\omega)$ (in units of $2e^2/h$) below the onset of interband transitions. (a) $\tilde{\Delta} < \varepsilon_F < \Delta$ and (b) $\varepsilon_F > \Delta$. We take $\Delta = 110$ meV. The shaded areas indicate hyperbolic regimes.

instead of the unique absorption edge $2\varepsilon_F$, characteristic of monolayer graphene. Below ω_- the JDOS vanishes, and above ω_+ it presents the typical linear behavior. Between ω_- and ω_+ the behavior is no longer linear, and globally, the JDOS displays a behavior which resembles that of the ungapped 8-*Pmmn* borophene [21]. (3) In contrast, when the Fermi level lies in the indirect zone, the JDOS displays a set of three Van Hove singularities (at 2Δ and $\hbar\omega_\pm$) and a significant overall size reduction due to a drastic shrinking of the momentum space available for direct transitions, caused by the indirect nature of the gap. In the same way, the intraband spectral weight is also anisotropic with a nonlinear dependence on the Fermi energy [24].

These spectral characteristics reveal that the intraband and interband contributions to the optical conductivity tensor $\sigma_{ij}(\omega)$ can be strongly modified by locating the Fermi level properly [37]. This offers the opportunity to control the form of propagation of surface electromagnetic modes. In particular, as we will see below, the conditions for hyperbolic plasmons become accessible. As is well known [1,3,38], a 2D material can support the hyperbolic dispersion relation of plasmons when $\text{Im}[\sigma_{xx}(\omega)]\text{Im}[\sigma_{yy}(\omega)] < 0$. The combination of time-reversal symmetry and broken inversion symmetry of the model (1) leads to an anisotropic response [24], $\sigma_{ij}(\omega) = \delta_{ij}[\sigma_{xx}(\omega)\delta_{ix} + \sigma_{yy}(\omega)\delta_{iy}]$. Figure 2(a) shows the xx and yy components when the Fermi level lies in the indirect zone $\tilde{\Delta} < \varepsilon_F < \Delta$, as calculated from Kubo's formula [37]. A well-defined hyperbolic region of frequencies exists where the losses are negligible, below the onset 2Δ of interband transitions and above the Drude peak. A hyperbolic region also appears for $\varepsilon_F > \Delta$, as can be seen in Fig. 2(b), with its width narrowing as Δ/ε_F approaches unity.

It is interesting to note that for a system with $\Delta \geqslant 0$ and $\gamma = 0$, the sign change of the imaginary parts of the longitudinal conductivities occurs at exactly the same frequency, and therefore, $\text{Im}[\sigma_{xx}(\omega)]\text{Im}[\sigma_{yy}(\omega)] \geqslant 0$ in the whole frequency range [Fig. 3(a)]. On the other hand, when only tilting is present, $\Delta = 0$ and $\gamma \neq 0$, the condition for hyperbolicity is satisfied but only above the onset for interband absorption [Fig. 3(b)], implying damped hyperbolic modes.

The calculations reveal that only the simultaneous presence of mass and tilting provides a way to asymmetrically
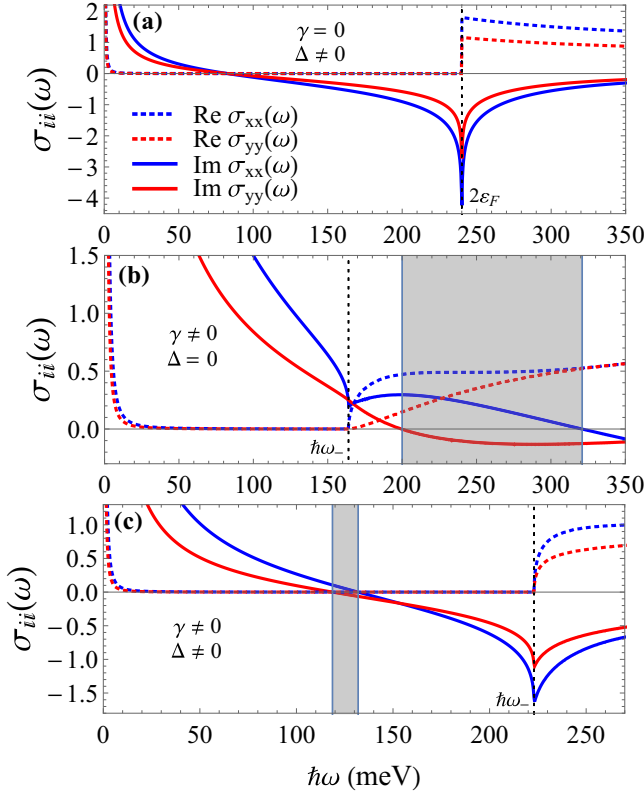
FIG. 3. Optical conductivities σ_{xx} and σ_{yy} (in units of $2e^2/h$) for Dirac cones with (a) gap, (b) tilt, and (c) gap and tilt. The shaded zones indicate the hyperbolic regimes. For (a) and (c) we take $\Delta = 110$ meV and $\varepsilon_F > \Delta$. The vertical dashed line denotes the onset $\hbar\omega_-$ of interband transitions in each case; it is blueshifted when a gap is introduced in the tilted system.

change the magnitude of the interband response versus the (positive) intraband contribution to $\text{Im}[\sigma_{ii}]$ in order to fulfill the hyperbolicity condition in a spectral region of low loss. For $\varepsilon_F > \Delta$, the opening of a gap in the tilted system cause a blueshift of the absorption edge $\hbar\omega_-$, increasing the frequency region between the Drude absorption and Landau damping [Fig. 3(c)]. This is in contrast to the gapless case, in which the onset for interband transitions can be arbitrarily small as $\varepsilon_F \to 0$, as in monolayer graphene or borophene 8-$Pmmn$ [21]. Similarly, when $\tilde{\Delta} < \varepsilon_F < \Delta$, a threshold of 2Δ appears for single-particle excitations, which also left spectral space for undamped hyperbolic plasmons.

The dispersion relation of surface waves localized in the z direction and propagating along the direction of the wave vector $\mathbf{q} = q_x\hat{\mathbf{x}} + q_y\hat{\mathbf{y}} = q(\cos\phi\hat{\mathbf{x}} + \sin\phi\hat{\mathbf{y}})$ on the xy plane is given by [2,38,39] $\tilde{\sigma}_{xx}(q_x^2 - k_0^2) + \tilde{\sigma}_{yy}(q_y^2 - k_0^2) = ik_0\kappa[1 + 4\pi^2\tilde{\sigma}_{xx}\tilde{\sigma}_{yy}]/2\pi$, written in terms of the dimensionless conductivity components $\tilde{\sigma}_{ii} = \sigma_{ii}/c$, where $k_0 = \omega/c$. The out-of-plane component of the plasmon wave vector is $q_z = i\kappa$, $\kappa(\omega) = \sqrt{q_x^2 + q_y^2 - k_0^2}$, where κ^{-1} measures the penetration depth of the evanescent mode into the neighboring media, which we assume to be vacuum for the sake of simplicity. When the power absorption is small, such that $\text{Re}[\sigma_{ii}(\omega)] \approx 0$, the dispersion relation reduces to a real equation. For a given frequency, this corresponds to a fourth-
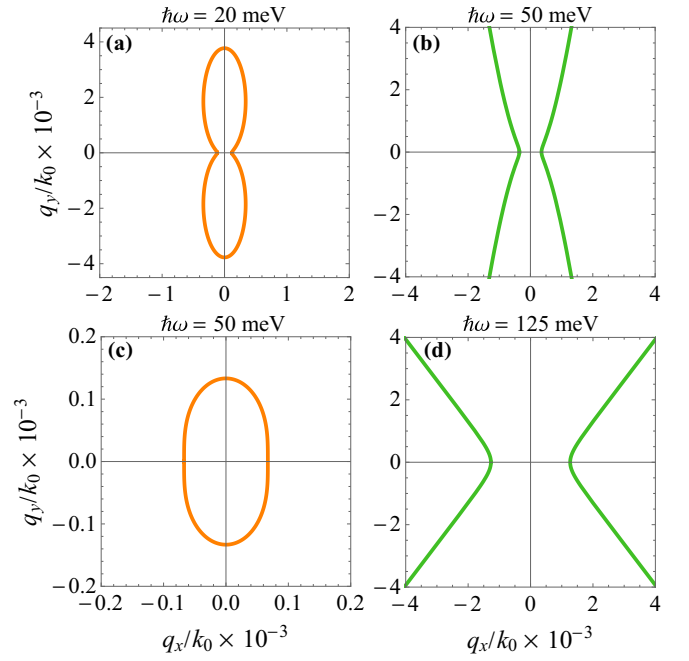

FIG. 4. Isofrequency contours $\omega(q_x, q_y) = $ const illustrating the plasmon propagation when (a) and (b) $\tilde{\Delta} < \varepsilon_F < \Delta$ and (c) and (d) $\varepsilon_F > \Delta$. The closed (open) curves correspond to a frequency lying outside (inside) the hyperbolic regions displayed in Fig. 2.

degree algebraic curve, whose gradient vector field defines the direction of energy propagation. Figure 4 illustrates the plasmon modes in $\mathbf{q}$ space for the cases shown in Fig. 2 at frequencies lying inside or outside a hyperbolic region. Given that $q_x, q_y \gg k_0$, the dispersion relation becomes well described by the expression

$$\frac{q_x^2}{\tilde{\sigma}_{yy}''(\omega)} + \frac{q_y^2}{\tilde{\sigma}_{xx}''(\omega)} = 2\pi k_0 q\{[4\pi^2\tilde{\sigma}_{xx}''(\omega)\tilde{\sigma}_{yy}''(\omega)]^{-1} - 1\}, \quad (4)$$

where $\tilde{\sigma}_{ii}'' \equiv \text{Im}[\tilde{\sigma}_{ii}(\omega)]$.

We can identify the characteristic properties associated with hyperbolic propagation [4,38]. Closed quasielliptic contours are obtained whenever $\text{Im}[\sigma_{xx}(\omega)]\text{Im}[\sigma_{yy}(\omega)] > 0$ (or $\text{Det}\{\text{Im}(\sigma_{ij})\} > 0$, given that $\sigma_{xy} = \sigma_{yx} = 0$), elongated along the smallest σ_{ii}; otherwise, hyperbolic branches are obtained, with asymptotes having slopes $\tan\theta = \pm\sqrt{-\text{Im}\,\sigma_{xx}(\omega)/\text{Im}\,\sigma_{yy}(\omega)}$. The group velocity points mainly along the directions $\mp\sqrt{-\text{Im}\,\sigma_{yy}(\omega)/\text{Im}\,\sigma_{xx}(\omega)}$, normal to the asymptotes, and large wave vectors can be supported, indicating a high degree of directionality and localization. This contrasts with the purely anisotropic case (closed curves) in which there is propagation in all directions, although less confinement of the mode. The topology (closed vs open isofrequency contours) and the direction of the plasmon propagation can be manipulated not only by changing the exciting frequency but also by varying only the position of the Fermi energy [Figs. 4(b) and 4(c)].

Note that using 8-$Pmmn$ borophene as a reference, all the parameters in the model (1) are fixed, with the exception of the magnitude of the mass Δ. This is in contrast to the minimal model considered in Ref. [4], where six parameters
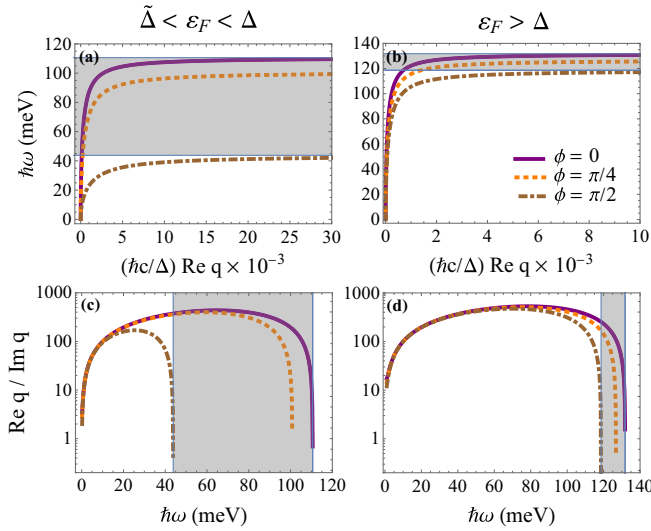
FIG. 5. (a) and (b) Frequency-momentum relation and (c) and (d) inverse of losses of the collectives modes for several propagation angles when $\tilde{\Delta} < \varepsilon_F < \Delta$ and $\varepsilon_F > \Delta$. Hyperbolic regions (in gray) correspond to those in Fig. 2.

were varied, using multilayer black phosphorus as the model candidate for the anisotropic 2D intrinsic material supporting hyperbolic modes. In our case, the calculated conductivity response cannot be effectively parametrized as in Ref. [4]. Moreover, we found that even for isotropic velocity, $v_x = v_y$, the tilting and the indirect nature of the gap along the k_y direction provide sufficient anisotropy to the system, while the introduction of mass leads to important modifications of the interband contribution as mentioned above. The joint effect of these two elements is enough to produce an interplay of the intraband and interband excitations capable of making the appearance of hyperbolicity of plasmon propagation possible, without any further material parameters.

Figures 5(a) and 5(b) display the surface plasmon dispersion for different angles of propagation ϕ at the same two positions of the Fermi level as in Fig. 2. The increasing density of states of modes as the dispersion curve enters the zone of hyperbolicity reflects the increasing spatial confinement. Figures 5(c) and 5(d) show the plasmon losses as the plasmon propagates within the surface along several directions ϕ. For $\phi = \pi/2$, the dispersion relation has a solution for frequencies below and up to the lower bound of the hyperbolic zone, as the existence of closed isofrequency contours illustrates [Figs. 4(a) and 4(c)]. For smaller ϕ, the solution enters a hyperbolic region eventually and will present a frequency cutoff ω_c defined by the condition that the decreasing slope (as ω increases) of the asymptote (see Fig. 2) finally match the direction ϕ, that is, the equation $\theta(\omega_c) = \phi$. For $\phi = 0$, ω_c is given by $\mathrm{Im}[\sigma_{xx}(\omega_c)] = 0$, which corresponds to the higher border of the hyperbolic zone. For $\phi = \pi/4$ the cutoff is redshifted because the frequency dominion available to reach the condition $\theta(\omega_c) = \phi$ is reduced. As $\phi \to \pi/2$, the solution cutoff approaches the frontier between elliptical and hyperbolical propagation, as $\mathrm{Im}[\sigma_{yy}(\omega)] \to 0^-$. On the other hand, at low frequencies the losses increase due to the intraband absorption. It is interesting to note that the propaga-

tive losses reach their minimum within the hyperbolic zone when $\tilde{\Delta} < \varepsilon_F < \Delta$ and within an elliptic zone when $\varepsilon_F > \Delta$. Thus, the system can support well-defined, highly directional hyperbolic plasmons. In particular, at a given frequency, the position of the Fermi level allows us to tune between purely anisotropic and hyperbolic propagation. According to Hamiltonian (1) and from previous knowledge of a nominal gap, one might think that the condition $\varepsilon_F < \Delta$ implies that hyperbolic propagation is impossible because of the absence of intraband transitions. However, as Fig. 5(c) shows, the propagation of hyperbolic plasmon is still possible because of the appearance of the indirect zone. This suggests that the Fermi energy dependence of the transitions illustrated in Fig. 5 is a clear indication of the presence of tilt and mass in the system.

There is a proposal to generate contrasting gaps in 2D Dirac materials using magnetic impurities [40,41]. We have also performed calculations considering these valley-dependent gaps. In this situation, the additional breaking of the time-reversal symmetry leads to a more complex spectral behavior of the optical response, given the extra possibilities for the position of the Fermi level and the associated spectrum of allowed excitations [24]. As a consequence, similar topological transitions in the form of collective mode propagation, like those described above, have been found with extended tunability.

Two effects ignored in this theoretical treatment can limit the observation of hyperbolic plasmons and the features described in this Letter, namely, nonlocality and finite-temperature effects. The former becomes relevant for plasmons with large spatial momentum q, like those involved in Figs. 4(b) and 4(d). However, hyperbolas with smaller wave vectors are obtained by increasing the degree of anisotropy. We found that the "size" of the hyperbolic curves displays a sensitive dependence on the material parameters used; for larger values of v_x, v_y, or $|v_x - v_y|$ or for larger values of tilting γ (like in WTe$_2$ [35]), the hyperbolas involve q/k_0 of the order of hundreds (comparable to the values reported for black phosphorus [13]) instead of thousands. However, some remarks are in order about the effects of spatial dispersion. In the tilted and gapped α-(BEDT-TTF)$_2$I$_3$ material, the Fermi velocity is about one order of magnitude smaller than that of graphene, which would imply a larger wave vector cutoff imposed by the spatial nonlocality. On the other hand, the impact of nonlocal effects on the hyperbolic propagation reported in Ref. [13] is applicable to a few layers of black phosphorus, including a quadratic term $\sim k^2$ in its low-energy Hamiltonian. Thus, it is unclear to what extent the nonlocality will influence the propagation and losses of the hyperbolic plasmons in our Dirac system. Even if such effects drastically limit their localization and directionality, one could expect at most a behavior similar to that of black phosphorus, in which the hyperbolic topology changes to a canalization regime, which is also of technological interest. The inclusion of nonlocality in our system deserves a proper investigation, which is beyond the scope of the present work. We hope our findings stimulate further exploration.

Finite-temperature effects will be irrelevant at low enough temperature $k_B T \ll \varepsilon_F, \Delta$. For other cases, we can estimate the effects of finite temperature on the propagative losses by

comparing them with gapped graphene, given that the overall sizes of the Im$\sigma_{ii}(\omega)$ spectra are similar. Following the usual thermal-convolution path [42,43] to calculate $\sigma_{ij}(\omega, T)$, it is found that Re(q)/Im(q) decreases by about an order of magnitude at room temperature for gapped graphene. Assuming the same for our tilted system, one might expect a reduction of about the same order of magnitude in the propagation length of the plasmons at room temperature.

We remark, however, that despite all these possible reducing effects, well-defined natural hyperbolic plasmon propagation, involving large wave vectors, was recently experimentally demonstrated in the far-IR range in thin films of the transition metal dichalcogenide WTe$_2$ at low temperatures (10–20 K) [6]. Since the $\mathbf{k} \cdot \mathbf{p}$ model Hamiltonian for low-lying excitations for this material [35] in its $1T'$ phase is similar to Eq. (1), this system becomes a platform where our theoretical predictions can be tested.

In summary, we have shown how an anisotropic 2D system with broken inversion and particle-hole symmetries can support well-defined, highly collimated, hyperbolic surface electromagnetic modes in the terahertz range. In particular, simultaneous mass *and* tilt lead to indirect gaps along the tilting direction, an additional source of anisotropy that substantially modifies the interband contribution to the optical response. Consequently, regions of hyperbolicity arise for the exciting frequency, tunable by the appropriate location of the Fermi level or the magnitude of the tilting. This mechanism differs from those reported for natural hyperbolic 2D systems like black phosphorus or some transition metal dichalcogenides like WTe$_2$. The characteristic topological transitions between closed and open forms of plasmon propagation suggest an optical signature of the simultaneous occurrence of tilt and mass. For typical material parameters, such as those involved in gapped graphene, 8-*Pmmn* borophene, α-(BEDT TTF)$_2$I$_3$, and WTe$_2$, the hyperbolic plasmons in our model lie in the range of a few tens of terahertz. Such a frequency range coincides with the one explored with far-infrared absorption spectroscopy in a recent experimental confirmation of hyperbolic plasmons in WTe$_2$ [6]. As in graphene plasmonics [44–46], one might expect that the current tools of far-infrared spectroscopy or near-field optical scattering techniques, which allow excitation with high values of the in-plane wave vectors, should be applicable for probing the hyperbolic propagation we report. Although motivated by systems like 8-*Pmmn* borophene, α-(BEDT-TTF)$_2$I$_3$, and WTe$_2$, our study should have relevance for the optical properties of anisotropic atomically thin materials.

[1] T. Low, A. Chaves, J. D. Caldwell, A. Kumar, N. X. Fang, P. Avouris, T. F. Heinz, F. Guinea, L. Martin-Moreno, and F. Koppens, Polaritons in layered two-dimensional materials, Nat. Mater. **16**, 182 (2017).

[2] A. Nemilentsau, T. Low, and G. Hanson, Chiral and hyperbolic plasmons in novel 2D materials, in *Carbon-Based Nanoelectromagnetics*, edited by A. Maffucci, S. Maksimenko, and Y. Svirko, Nanophotonics Series (Elsevier, Amsterdam, 2019), pp. 119–138.

[3] J. S. Gomez-Diaz, M. Tymchenko, and A. Alù, Hyperbolic Plasmons and Topological Transitions over Uniaxial Metasurfaces, Phys. Rev. Lett. **114**, 233901 (2015).

[4] A. Nemilentsau, T. Low, and G. Hanson, Anisotropic 2D Materials for Tunable Hyperbolic Plasmonics, Phys. Rev. Lett. **116**, 066804 (2016).

[5] J. Sun, N. M. Litchinitser, and J. Zhou, Indefinite by nature: From ultraviolet to terahertz, ACS Photonics **1**, 293 (2014).

[6] C. Wang, S. Huang, Q. Xing, Y. Xie, C. Song, F. Wang, and H. Yan, Van der Waals thin films of WTe$_2$ for natural hyperbolic plasmonic surfaces, Nat. Commun. **11**, 1158 (2020).

[7] Z. Torbatian, D. Novko, and R. Asgari, Tunable Low-Loss Hyperbolic Plasmon Polaritons in a T$_d$-WTe$_2$ Single Layer, Phys. Rev. Appl. **14**, 044014 (2020).

[8] H. Wang and T. Low, Hyperbolicity in two-dimensional transition metal ditellurides induced by electronic bands nesting, Phys. Rev. B **102**, 241104(R) (2020).

[9] S. Edalati-Boostan, C. Cocchi, and C. Draxl, MoTe$_2$ as a natural hyperbolic material across the visible and the ultraviolet region, Phys. Rev. Materials **4**, 085202 (2020).

[10] S. Guan, S. Y. Huang, Y. Yao, and S. A. Yang, Tunable hyperbolic dispersion and negative refraction in natural electride materials, Phys. Rev. B **95**, 165436 (2017).

[11] Z. Zheng, N. Xu, S. L. Oscurato, M. Tamagnone, F. Sun, Y. Jiang, Y. Ke, J. Chen, W. Huang, W. L. Wilson, A. Ambrosio, S. Deng, and H. Chen, A mid-infrared biaxial hyperbolic van der Waals crystal, Sci. Adv. **5**, eaav8690 (2019).

[12] A. Ebrahimian and R. Asgari, Natural hyperbolicity in layered hexagonal crystal structures, Phys. Rev. B **103**, 035425 (2021).

[13] D. Correas-Serrano, J. S. Gomez-Diaz, A. A. Melcon, and A. Alù, Black phosphorus plasmonics: Anisotropic elliptical propagation and nonlocality-induced canalization, J. Opt. **18**, 104006 (2016).

[14] E. van Veen, A. Nemilentsau, A. Kumar, R. Roldán, M. I. Katsnelson, T. Low, and S. Yuan, Tuning two-dimensional hyperbolic plasmons in black phosphorus, Phys. Rev. Appl. **12**, 014011 (2019).

[15] M. Dehdast, Z. Valiollahi, M. Neek-Amal, B. Van Duppen, F. Peeters, and M. Pourfath, Tunable natural terahertz and mid-infrared hyperbolic plasmons in carbon phosphide, Carbon **178**, 625 (2021).

[16] Z. Torbatian, D. Novko, and R. Asgari, Hyperbolic plasmon modes in tilted Dirac cone phases of borophene, Phys. Rev. B **104**, 075432 (2021).

[17] J. Zhao, W. Wu, J. Zhu, Y. Lu, B. Xiang, and S. A. Yang, Highly anisotropic two-dimensional metal in monolayer MoOCl$_2$, Phys. Rev. B **102**, 245419 (2020).

[18] Y. Shao, A. Sternbach, B. Kim, A. Rikhter, X. Xu, U. De Giovannini, R. Jing, S. H. Chae, Z. Sun, Y. L. Zhu, Z. Mao,

J. Hone, R. Queiroz, A. Millis, P. Schuck, A. Rubio, M. Fogler, and D. Basov, Hyperbolic plasmons propagate through a nodal metal (unpublished).

[19] M. B. Schilling, L. M. Schoop, B. V. Lotsch, M. Dressel, and A. V. Pronin, Flat Optical Conductivity in ZrSiS due to Two-Dimensional Dirac Bands, Phys. Rev. Lett. **119**, 187401 (2017).

[20] S. Ahn and S. Das Sarma, Theory of anisotropic plasmons, Phys. Rev. B **103**, L041303 (2021).

[21] S. Verma, A. Mawrie, and T. K. Ghosh, Effect of electron-hole asymmetry on optical conductivity in 8-*Pmmn* borophene, Phys. Rev. B **96**, 155418 (2017).

[22] E. Uykur, W. Li, C. A. Kuntscher, and M. Dressel, Optical signatures of energy gap in correlated Dirac fermions, npj Quantum Mater. **4**, 19 (2019).

[23] K. Yoshimura, M. Sato, and T. Osada, Experimental confirmation of massive Dirac fermions in weak charge-ordering state in α-(BEDT-TTF)$_2$I$_3$, J. Phys. Soc. Jpn. **90**, 033701 (2021).

[24] M. A. Mojarro, R. Carrillo-Bastos, and J. A. Maytorena, Optical properties of massive anisotropic tilted Dirac systems, Phys. Rev. B **103**, 165415 (2021).

[25] Y. Betancur-Ocampo, E. Díaz-Bautista, and T. Stegmann, Valley-dependent time evolution of coherent electron states in tilted anisotropic Dirac materials, Phys. Rev. B **105**, 045401 (2022).

[26] P. Kapri, B. Dey, and T. K. Ghosh, Valley caloritronics in a photodriven heterojunction of Dirac materials, Phys. Rev. B **102**, 045417 (2020).

[27] H. Rostami and V. Juričić, Probing quantum criticality using nonlinear Hall effect in a metallic Dirac system, Phys. Rev. Research **2**, 013069 (2020).

[28] M. O. Goerbig, J.-N. Fuchs, G. Montambaux, and F. Piéchon, Tilted anisotropic Dirac cones in quinoid-type graphene and $\alpha-$(BEDT-TTF)$_2$I$_3$, Phys. Rev. B **78**, 045415 (2008).

[29] J. Sári, C. Tőke, and M. O. Goerbig, Magnetoplasmons of the tilted anisotropic Dirac cone material α-(BEDT-TTF)$_2$I$_3$, Phys. Rev. B **90**, 155446 (2014).

[30] S. Rostamzadeh, İ. Adagideli, and M. O. Goerbig, Large enhancement of conductivity in Weyl semimetals with tilted cones: Pseudorelativity and linear response, Phys. Rev. B **100**, 075438 (2019).

[31] A. D. Zabolotskiy and Y. E. Lozovik, Strain-induced pseudomagnetic field in the Dirac semimetal borophene, Phys. Rev. B **94**, 165403 (2016).

[32] K. Kajita, Y. Nishio, N. Tajima, Y. Suzumura, and A. Kobayashi, Molecular Dirac fermion systems – Theoretical and experimental approaches, J. Phys. Soc. Jpn. **83**, 072002 (2014).

[33] M. Hirata, K. Ishikawa, K. Miyagawa, M. Tamura, C. Berthier, D. Basko, A. Kobayashi, G. Matsuno, and K. Kanoda, Observation of an anisotropic Dirac cone reshaping and ferrimagnetic spin polarization in an organic conductor, Nat. Commun. **7**, 12666 (2016).

[34] T. Osada and A. Kiswandhi, Possible current-induced phenomena and domain control in an organic Dirac fermion system with weak charge ordering, J. Phys. Soc. Jpn. **89**, 103701 (2020).

[35] S. Nandy and D. A. Pesin, Low-energy effective theory and anomalous Hall effect in monolayer WTe$_2$, SciPost Phys. **12**, 120 (2022).

[36] Z.-Q. Wang, T.-Y. Lü, H.-Q. Wang, Y. P. Feng, and J.-C. Zheng, Band gap opening in 8-pmmn borophene by hydrogenation, ACS Appl. Electron. Mater. **1**, 667 (2019).

[37] See Supplemental Material at http://link.aps.org/supplemental/10.1103/PhysRevB.105.L201408 for details of the full expressions of the optical conductivity tensor for a generic two-band model, and the corresponding intra- and interband contributions for a massive anisotropic tilted two-dimensional Dirac system.

[38] J. S. Gomez-Diaz, M. Tymchenko, and A. Alù, Hyperbolic metasurfaces: Surface plasmons, light-matter interactions, and physical implementation using graphene strips, Opt. Mater. Express **5**, 2313 (2015).

[39] G. W. Hanson, Dyadic Green's function for an anisotropic, non-local model of biased graphene, IEEE Trans. Antennas Propag. **56**, 747 (2008).

[40] A. Hill, A. Sinner, and K. Ziegler, Valley symmetry breaking and gap tuning in graphene by spin doping, New J. Phys. **13**, 035023 (2011).

[41] B. R. Matis, B. H. Houston, and J. W. Baldwin, Evidence for spin glass ordering near the weak to strong localization transition in hydrogenated graphene, ACS Nano **10**, 4857 (2016).

[42] A. Iurov, G. Gumbs, D. Huang, and V. M. Silkin, Plasmon dissipation in gapped graphene open systems at finite temperature, Phys. Rev. B **93**, 035404 (2016).

[43] A. Iurov, G. Gumbs, D. Huang, and G. Balakrishnan, Thermal plasmons controlled by different thermal-convolution paths in tunable extrinsic Dirac structures, Phys. Rev. B **96**, 245403 (2017).

[44] Z. Fei, G. O. Andreev, W. Bao, L. M. Zhang, A. S. McLeod, C. Wang, M. K. Stewart, Z. Zhao, G. Dominguez, M. Thiemens, M. M. Fogler, M. J. Tauber, A. H. Castro-Neto, C. N. Lau, F. Keilmann, and D. N. Basov, Infrared nanoscopy of Dirac plasmons at the graphene-SiO$_2$ interface, Nano Lett. **11**, 4701 (2011).

[45] J. Chen, M. Badioli, P. Alonso-Gonzalez, S. Thongrattanasiri, F. Huth, J. Osmond, M. Spasenović, A. Centeno, A. Pesquera, P. Godignon, A. Z. Elorza, N. Camara, F. J. García de Abajo, R. Hillenbrand, and F. H. L. Koppens, Optical nano-imaging of gate-tunable graphene plasmons, Nature (London) **487**, 77 (2012).

[46] T. J. Constant, S. M. Hornett, D. E. Chang, and E. Hendry, All-optical generation of surface plasmons in graphene, Nat. Phys. **12**, 124 (2016).